A Simulation Framework for Magnetic Continuum Robots

Roland Dreyfus[1], Quentin Boehler[1] and Bradley J. Nelson[1]

***Abstract*—Remote magnetic navigation is a technology used to robotically steer magnetic medical instruments, such as magnetic catheters and guidewires, for minimally invasive surgery. The ability to model and simulate the behavior of these magnetic instruments in complex anatomies is important for their clinical use in many ways. Simulation frameworks can improve their design, characterization, and automatic control capabilities, as well as provide training simulators for physicians. In this work we introduce a new simulation framework that accounts for both magnetic actuation and interactions forces with meshed collision models. The simulations are validated experimentally in planar rigid models using a pre-clinical electromagnetic navigation system. We also demonstrate the use of our framework to build training simulators for two endovascular navigation tasks including the exploration of the aortic arch and the internal carotid artery.**

***Index Terms*—Surgical Robotics: Steerable Catheters/Needles; Simulation and Animation; Modeling, Control, and Learning for Soft Robots**

I. Introduction

REMOTE magnetic navigation (RMN) is a technology in which magnetic fields are used to wirelessly navigate devices containing magnetic material [1]. Magnetic continuum robots (m-CRs) actuated by RMN, such as magnetic catheters and guidewires, are of increasing interest for several minimally invasive surgeries including cardiac ablations [2] and neurovascular interventions [3]. An m-CR is composed of permanent magnets [4] or magnetic particles [5], [6] embedded along a flexible body in which deflection is induced by the torques produced on the magnets by externally generated magnetic fields. These magnetic fields can be generated with an electromagnetic navigation system (eMNS) [7]. This distal actuation allows an m-CR to generate tip forces while having a soft body, making it safe for interactions with human tissue.

The ability to model and simulate the behavior of minimally invasive flexible tools in complex anatomies is central for their clinical use [8]. Simulators are useful tools for characterizing and evaluating new instruments and for aiding in their design process [9]. When pre- or intraoperative anatomical data are available, simulators can also be used for the automatic control of the instrument [10], and for planning the procedure [11].

Manuscript received: February, 24, 2022; Revised May, 13, 2022; Accepted June, 13, 2022.

This paper was recommended for publication by Editor Pietro Valdastri upon evaluation of the Associate Editor and Reviewers' comments. This work was supported by the Swiss National Science Foundation through grant number 200020B_185039, the ITC-InnoHK funding, and the ERC Advanced Grant 743217 Soft Micro Robotics (SOMBOT).

[1]Multi-Scale Robotics Lab, ETH Zurich dreyfusr@ethz.ch

Digital Object Identifier (DOI): see top of this page.

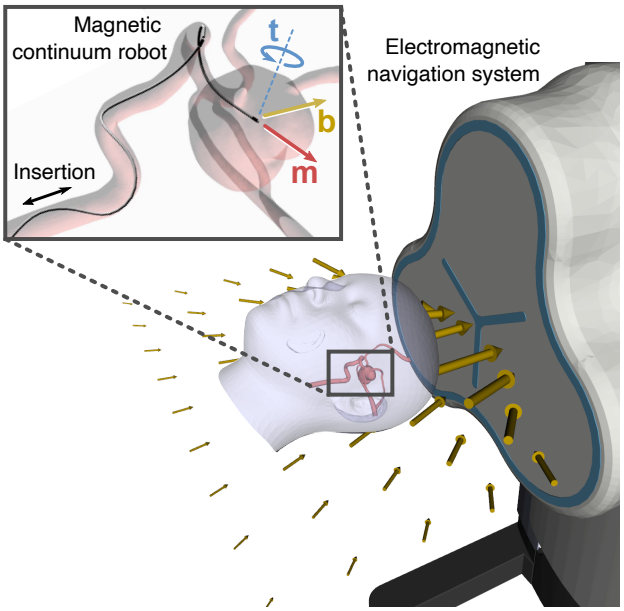

Fig. 1. Overview of the simulation framework in RViz. The magnetic fields generated by the electromagnetic navigation system are represented by the yellow arrows on a discretized 2d grid. The magnetic continuum robot is inserted from its proximal side by an advancer. A magnet of dipole moment $\mathbf{m}$ embedded along the flexible body of the robot experiences a torque $\mathbf{t} = \mathbf{m} \times \mathbf{b}$ when submitted to a magnetic field $\mathbf{b}$.

The training of physicians can also be significantly improved by the use of realistic endovascular simulators [12].

The modeling and simulation of m-CRs received sustained research attention over the past fifteen years. Because of the different steering paradigms between magnetic and non-magnetic instruments, the simulator must incorporate additional physical laws to deal with the behavior of soft and hard magnetic materials. Models are based on constant curvature [13] and pseudo-rigid body modeling [14], Cosserat rod theory [4], and Euler-Bernoulli beam theory [15]. Numerical tools have also been used to analyse singularities and unstable behaviors of m-CRs [16]. More recently, several efforts proposed the use of finite elements models [17]–[19], which includes the consideration of tip contact force in the context of cardiac catheters [20]. However, these investigations are limited by the absence or simplicity of the collision environment in which the magnetic instruments are simulated. The introduction of the Simulation Open Framework Architecture (SOFA) [21] and its *BeamAdapter* plugin [22] constitutes a promising option to simulate m-CRs and their interaction forces with complex and soft anatomies. This framework has

already been successfully used for the automatic control of guidewires in neurovascular applications [23], [24], the design of patient-specific catheters in coronary angiography [9], and the development of training simulators for endovascular procedures [25], [26]. Though, these efforts are limited to applications using conventional, non-magnetically guided instruments.

In this work, we introduce a SOFA-based simulator that includes magnetic interactions to simulate the behavior of m-CRs in a variety of environments. We couple this simulator to a Robot Operating System (ROS) environment [27] to include magnetic models of an eMNS that generates non-homogeneous external magnetic fields [7]. We provide an experimental validation of our approach in planar rigid environments and show navigation tasks performed in simulated 3d anatomies.

II. Simulation framework

An overview of the simulation framework[1] is depicted in Fig. 1. The interface is realized with RViz and is composed of the models of the eMNS, the anatomical environment, and the m-CR.

A. Electromagnetic navigation system

The eMNS is modeled as a set of magnetic multipoles using the approach described in [28] where the currents $\mathbf{i} \in \mathbb{R}^{n_c}$ in the n_c coils composing the system are linearly mapped to the magnetic field $\mathbf{b}(\mathbf{p}) \in \mathbb{R}^3$ at any position $\mathbf{p}$ within the calibrated volume of the system using an actuation matrix $\mathbf{A}(\mathbf{p}) \in \mathbb{R}^{3\times n_c}$ so that

$$\mathbf{b}(\mathbf{p}) = \mathbf{A}(\mathbf{p})\ \mathbf{i} \tag{1}$$

The matrix $\mathbf{A}(\mathbf{p})$ sums the contribution of each electromagnet to the magnetic field as

$$\mathbf{b}(\mathbf{p}) = \begin{bmatrix}\mathbf{A}_1(\mathbf{p}) & \cdots & \mathbf{A}_j(\mathbf{p}) & \cdots & \mathbf{A}_{n_c}(\mathbf{p})\end{bmatrix} \begin{bmatrix} i_1 \\ \vdots \\ i_j \\ \vdots \\ i_{n_c} \end{bmatrix} \tag{2}$$

$\mathbf{A}_j(\mathbf{p})$ is the contribution of the j-th current i_j to the magnetic field at $\mathbf{p}$ based on a magnetic multipole expansion presented in [28].

B. Magnetic continuum robot

The mechanical behavior of the m-CR is modelled with the open source SOFA simulation framework [21] combined with the *BeamAdapter* plugin [22]. The framework uses a 1-dimensional FEM of the continuum robot based on Kirchhoff rod theory, where the robot is discretized into beam elements composed of n nodes. Contacts are solved with Lagrange multipliers upon collision detection.

[1]https://github.com/ethz-msrl/mCR_simulator (release v1.0.0)

C. Coupling the models

An m-CR is steered by remotely applying torques on the embedded magnets with the external magnetic field generated by the eMNS. The magnets are characterized by the magnetic moment $\mathbf{m}_i$ at the i-th node of the discretized m-CR with $i \in \{1 \dots n\}$. The external magnetic field $\mathbf{b}(\mathbf{p}_i)$ induces an external torque $\mathbf{t}_i$ on the magnet that tends to reduce the offset angle between $\mathbf{m}_i$ and $\mathbf{b}(\mathbf{p}_i)$. The torque exerted on the node i is given by the relationship

$$\mathbf{t}_i = \mathbf{m}_i \times \mathbf{b}(\mathbf{p}_i) \tag{3}$$

as also depicted in the close-up Fig. 1. At every time step, the position $\mathbf{p}_i$ of each magnet is extracted from the SOFA simulation and fed into the magnetic model (1), providing the magnetic field $\mathbf{b}(\mathbf{p}_i)$. The external torque is then computed using (3) and applied on the corresponding node in the simulator.

D. User interface

ROS is used for multi-threading and to interface the simulation modules. The built-in visualization plugin RViz and a dedicated graphical user interface serves as a visual interface to the user. For all manual steering, a Sony PS4 DualShock Wireless-Controller is used. It allows the user to control the insertion and retraction of the m-CR, and the magnetic field.

III. Experimental Validation

Our simulator is evaluated experimentally to validate the behaviour of the simulated robots compared to the real ones. In the experiment, we navigate the m-CR in different environments and record the magnetic field and advancer inputs provided by the user. The simulated m-CR is then calibrated based on a calibration sequence and navigated in open-loop in the simulated environments, using the recorded user inputs from the experiment. The m-CR behavior is compared qualitatively by comparing the overall behaviour and quantitatively by estimating the error in tip position and orientation. An overview of the experimental setup is shown in Fig. 3, and a block diagram of the system control during experiments and simulations in Fig. 4.

A. Electromagnetic navigation system

We use a system composed of $n_c = 3$ parallel coils arranged on a triangular base (see Fig. 3). The input currents that result

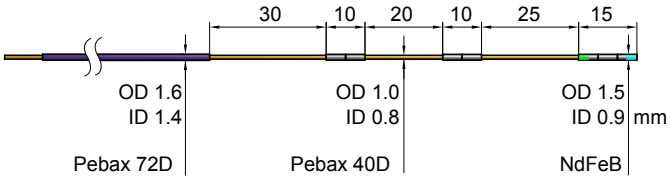

Fig. 2. m-CR used in the experimental validation. The m-CR has a rigid proximal and flexible distal section with three permanent ring magnets. The tip holds a green and blue color marker for optical tracking of the tip position and orientation.

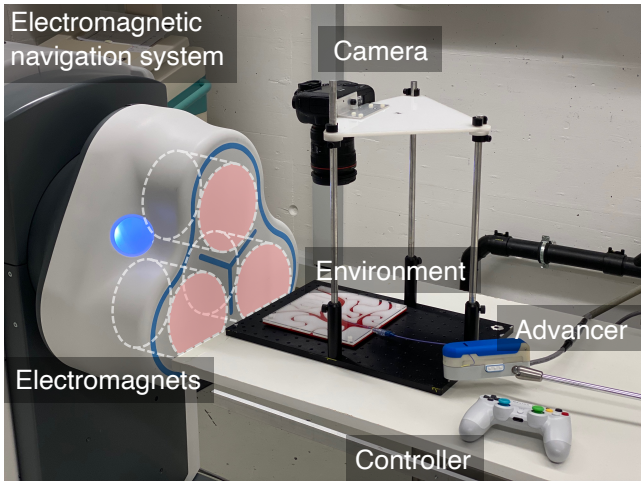

Fig. 3. Overview of the experimental validation setup.

in a magnetic field at $\mathbf{p}$ can be computed by solving (1) for $\mathbf{i}$ as [7]

$$\mathbf{i} = \mathbf{A}^{\dagger}(\mathbf{p})\mathbf{b}(\mathbf{p}) \tag{4}$$

where $\mathbf{A}^{\dagger}$ is the Moore-Penrose pseudoinverse of $\mathbf{A}$.

During m-CR navigation, the user changes the magnetic field $\mathbf{b}(\mathbf{p}_0)$ where $\mathbf{p}_0$ is the center of the calibrated volume of the eMNS, 200 mm away from the coils' surface. The magnetic field $\mathbf{b}(\mathbf{p}_0)$ can reach up to 25 mT in magnitude in any direction in three-dimensional space.

B. Magnetic continuum robot

An m-CR composed of two segments with different rigidity and embedding three magnets is used for this experimental validation (see Fig. 2). The m-CR has an outer diameter (OD) of 1.5 mm (4.5 Fr). Insertion and retraction is performed by applying an axial force f_{adv} on the proximal end. It is realized by coupling the m-CR to a remote controlled advancer unit, where the user controls the insertion speed v.

C. Environments

The instrument is navigated in planar, 4 mm high, rigid environments made from polyoxymethylene (POM) and poly(methyl methacrylate) (PMMA). The environments allow for simple experimental work and robust visual tracking of the m-CR tip. The m-CR can both move freely and collide with obstacles to adopt complex shapes (see Fig 5). The first environment has no obstacles and is used for calibration, the second environment is designed to resemble vasculature, and in the third environment, obstacles are freely arranged to provoke non-trivial situations. Each environment is centered around $\mathbf{p}_0$.

D. Visual tracking

Image feedback is provided with a Canon EOS 6D camera with a resolution of 1920 $\times$ 1080 pixels and is operated at 25 fps. The tip of the m-CR is equipped with a green and blue color marker. An image processing pipeline is used to extract the 2d tip position $\mathbf{p}_{tip,exp}$ and orientation $\mathbf{q}_{tip,exp}$ with respect to the environment. The video frames are converted into HSV color space to segment the color markers providing information on the markers positions, orientation, and distance from one another. To add robustness and avoid false detections, all detected markers that are too close or too far apart are discarded. All image processing steps are performed using OpenCV [29].

TABLE I
PARAMETERS OF THE SIMULATED M-CR.

Task	Design	Distal length [mm]	OD [mm]	ID [mm]	E_{dist} [MPa]	E_{prox} [MPa]
Validation	—	110	1.0	0.8	40	600
AA	Short Medium Long	14 34 54	1.33	0.8	21	170
ICA	Short Medium Long	10 30 40	0.7	0	500	20000

E. Simulation

The m-CR model is composed of 7 nodes on the distal section and a node density of 1.15 cm^{-1} on the proximal section. The visual model is based on a 1d regular grid with 4.0 mm spacing. The simulation uses a time step of 20 ms and a coefficient of friction of 0.01. The 3d magnetic field of the eMNS is modelled using the method described in section II-A. The simulations were performed on an Intel i5-4590 3.30 Hz computer processing unit (CPU) with 7.7 GB of random access memory (RAM).

F. Magnetic continuum robot calibration

A calibration sequence is performed in the obstacle-free environment to tune the simulation parameters. The calibration sequence is depicted in Fig. 5 under *Calibration*. Parameter tuning is performed by first fixing the remanence of the magnets and m-CR geometry, followed by sweeping the Young's moduli of the proximal stiff segment and the distal flexible segment by hand. Once the m-CR model is calibrated, the same parameters are used in the collision environments. The parameters that define the mechanical properties of the m-CR resulting from the parameter tuning are summarized in Table I under *Validation*.

G. Comparing experiment and simulation

After calibrating the simulated m-CR, the recordings of the experimental user inputs are used to actuate the simulated m-CR in open-loop in the simulated environments. The tip pose ($\mathbf{p}_{tip,sim}$ and $\mathbf{q}_{tip,sim}$) is extracted from the simulation and compared to the tracked pose from the experiments by calculating the errors between the two (see Fig. 5). The simulation runs at 18 Hz and the recorded data has a sampling rate of 25 Hz. To synchronize data points, the data are

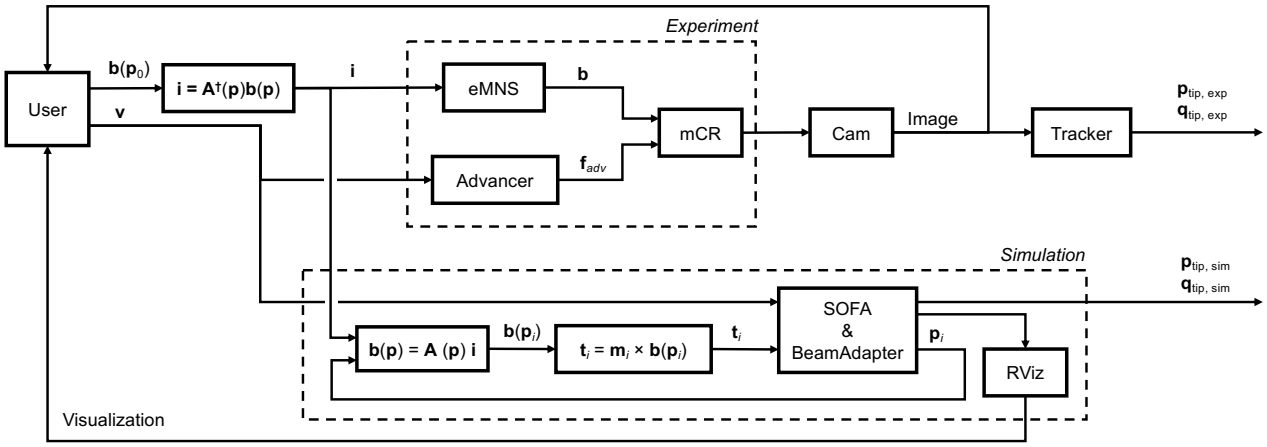

Fig. 4. Block diagram of the experiment and the simulation. The simulated mCR is actuated with the same user inputs as the real mCR.

resampled during postprocessing. The error in position is calculated by taking the Euclidean distance between points in the experiment and in the simulation at a given time. The angle error corresponds to the angle between the experimental and simulated tip pointing vectors. The position and orientation errors are evaluated during the entire navigation time T_{tot}. The average position error $\overline{e}_p$ and orientation error $\overline{e}_q$ taken across all error points of an entire navigation range from 5.1 to 6.8 mm and from 3.8 to 7.2 degrees. The errors at critical waypoints such as bifurcations and target end-points are presented in Table II.

IV. Applications

Our framework is used to build simulators for two realistic scenarios in endovascular interventions performed by neuroradiologists. The first scenario is the navigation in the aortic arch (AA), which is the gateway to the brain vessels in minimally invasive neurosurgery. The second is the exploration of the internal carotid artery (ICA), an intracranial vessel where aneurysms are commonly found [30].

We demonstrate simulated navigation tasks using two-magnet m-CR. The robots are composed of a magnet at the tip of a flexible distal section of Young's modulus E_{dist}, and a stiffer proximal section of Young's modulus E_{prox} (see Table I). The second magnet is placed at the junction between the two sections.

For each task, we record a first navigation performed by the user. These inputs are then replayed with different lengths of the distal flexible section in order to illustrate the influence of design parameters on the behavior of the robot (see Table I).

A. Aortic arch navigation

The results are illustrated in Fig. 6a. We use a type I AA model composed of the aorta and three supra-aortic vessels: the left subclavian artery (LSA), the left common carotid artery (LCC), and the brachiocephalic artery (BCA). This simulates a realistic task in which a catheter is placed in the AA or the supra-aortic vessels to perform roadmap and diagnostic angiographies by injecting a contrast agent through the catheter. We simulate a magnetic angiography catheter with a short, medium, and long distal section (see Table I). Magnets are 4 mm long with a remanence of 1.45 T, and with the same diameters as the robot. The catheter model is composed of 6 nodes on the distal section, and a node density of 0.6 cm^{-1} on the proximal section (variable inserted length). A visual model based on a 1d regular grid with 2.5 mm spacing is interpolated on the resulting nodes poses of the behavioral model. The simulation is run with a time step of 20 ms and a coefficient of friction of 0.02.

The figure illustrates navigation into the aorta and passing the tip into the BCA. The simulation captures different conformations of the flexible tip, when the catheter is shaped by the magnetic field and pushed further into the aorta. This includes the presence of inflexion points in the shape of the distal section as the latter becomes longer and collides with the aorta wall (see t = 15 s for the long tip).

B. Internal Carotid Artery exploration

The results are illustrated in Fig. 6b. We use a model of the ICA comprising a giant intracranial aneurysm and simulate a magnetic guidewire with a short, medium, and long distal section (see Table I). Magnets are 1 mm long with a remanence of 1.45 T and with the same diameters as the robot. The guidewire model is composed of 10 nodes on the distal section and a node density of 1.5 cm^{-1} on the proximal section. The visual model is based on a 1d regular grid with 0.3 mm spacing. The simulation uses a time step of 5 ms and a coefficient of friction of 0.3.

The different tools show different placement within the tortuous anatomy of the ICA depending on the tool design, which affect their contact on the vessel wall and the resulting friction forces. The short and long tip configuration show unfavourable behaviour such as kinking (Figure 6b Short tip) and buckling (Figure 6b Long Tip), which can be expected when instruments are excessively pushed while the distal tip is prevented from advancing [31]. The aneurysm can ultimately be reached with the medium tip after 4 min of navigation (see right of Fig. 6b). In this configuration, the simulation clearly

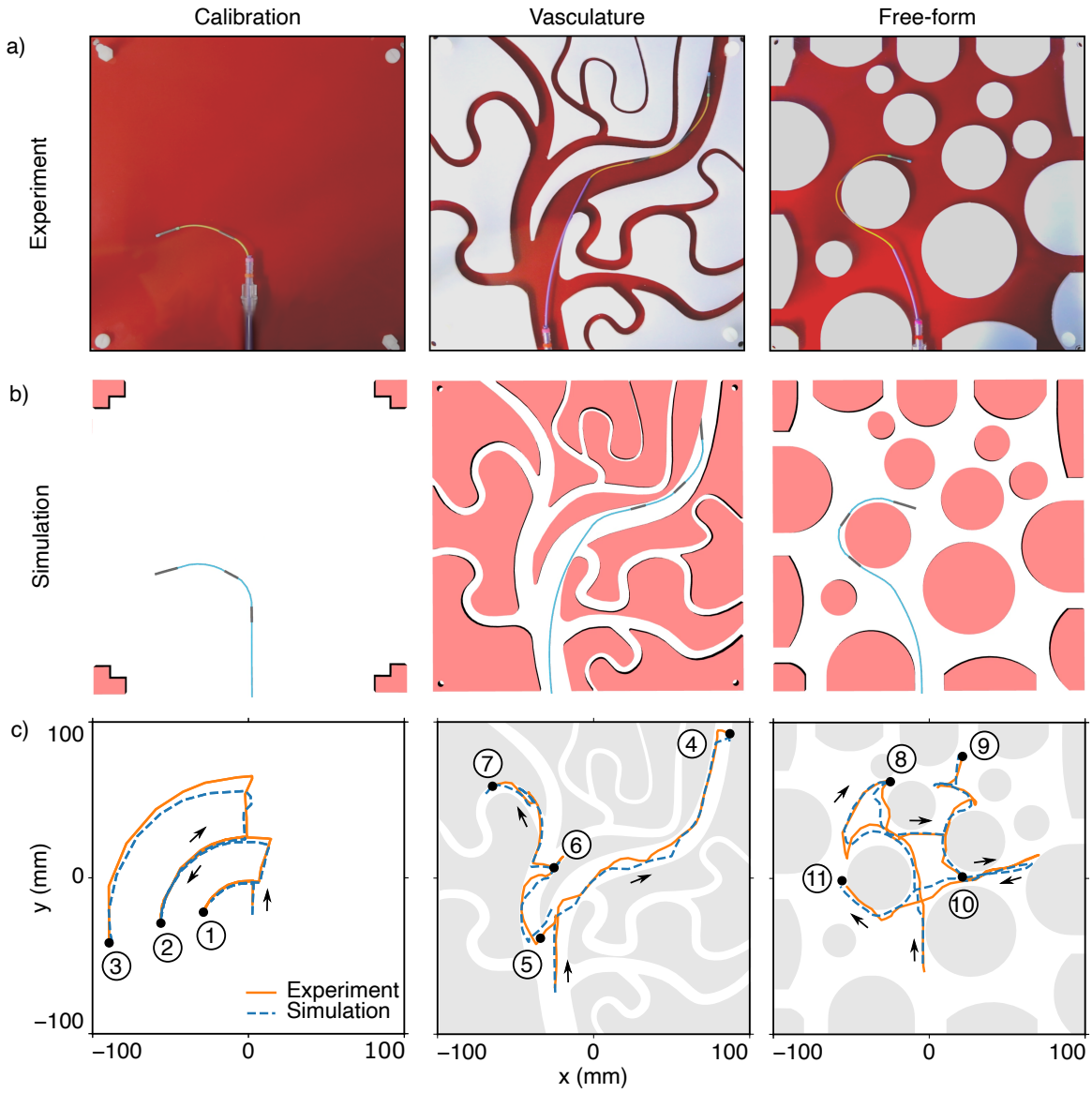

Fig. 5. Experimental validation of the m-CR simulator in planar environments. The simulated m-CR is first calibrated using a calibration sequence and then navigated in environments with obstacles and collisions.

shows the accumulated elastic energy in the proximal section of the tool due to the friction of the distal part inserted into the ICA. This behavior is well-known by neuroradiologists. It leads to unstable elastic behavior that constitute one of the main challenges of the procedure.

V. Discussion

The simulated m-CR showed similar behaviour to its physical counterpart used in our experiments. The average errors in position and angle in the different environments range from 5.1 to 6.8 mm and from 3.8 to 7.2 degrees, respectively. The errors can be attributed to experimental inaccuracies, timing sensitivity of the error measurement, and by the fact that the parameters were tuned by hand. Furthermore, errors can be caused by the general limitations of simulations where physical properties such as friction and material homogeneity are idealized and numerical inaccuracies can accumulate. The results from the experimental section confirm that the simulated m-CRs behave similarly to real m-CRs, even in situations with collisions and multiple contact points.

In the present work, we did not consider soft tissue deformations due to the general high flexibility of m-CRs. However, when stiff non-magnetic instruments are passed through highly tortuous vessels, the vessels can undergo large non-linear deformations. Furthermore, in the presence of high magnetic field gradients, m-CRs with particularly high magnetic volumes and very high flexibility can be moved by magnetic forces. To further bridge the reality gap, we will enhance the simulator by adding deformable anatomy modelling, include a model for magnetic forces based on the equations shown in [32], and implement a stereo tracking system to perform model-matching in 3d anatomical environments.

We demonstrate that the simulator can be used to analyze the behaviour of m-CRs in simulated anatomical environments

TABLE II
POSITION AND ORIENTATION ERROR BETWEEN THE REAL AND SIMULATED M-CR.

Environment	Way-point number	Way-point type	T [s]	$e_p(t=T)$ [mm]	$e_q(t=T)$ [°]	T_{tot} [s]	$\bar{e}_p$ [mm]	$\bar{e}_q$ [°]
Calibration	1	end-point	5.7	9.2	19.5	20.7	6.8	7.0
	2	end-point	12.8	1.9	6.1			
	3	end-point	20.7	2.0	3.6			
Vasculature	4	bifurcation	14.9	0.6	3.1	48.6	4.8	3.8
	5	bifurcation	30.0	4.9	1.9			
	6	end-point	37.1	1.1	1.3			
	7	end-point	48.6	5.0	3.0			
Free-form	8	end-point	10.0	2.4	0.2	46.0	5.1	7.2
	9	end-point	24.7	2.6	0.9			
	10	bifurcation	32.8	1.5	7.4			
	11	end-point	46.1	3.6	2.7			

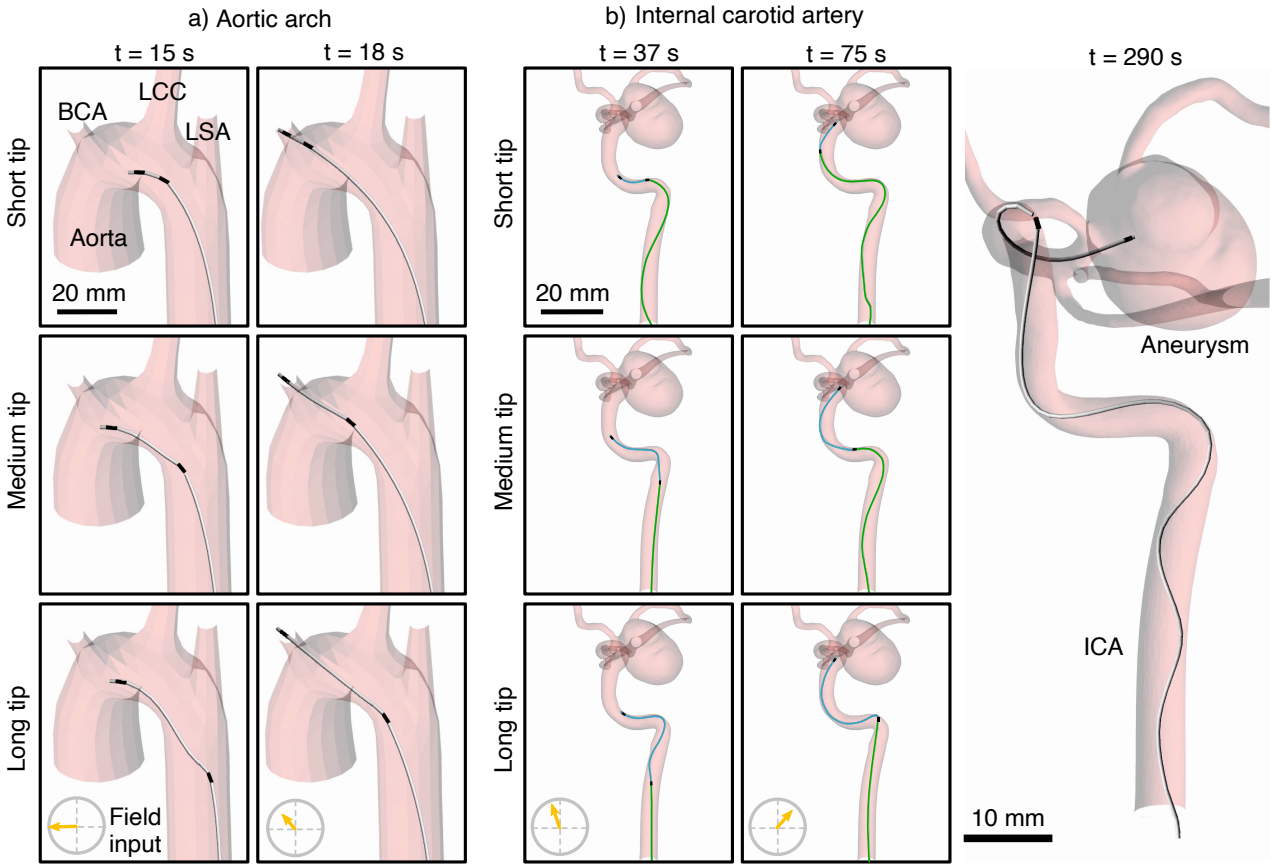

Fig. 6. Applications of the simulator framework to endovascular navigation tasks. a) Navigation in the aortic arch, and b) exploration of the internal carotid artery toward a giant intracranial aneurysm. The simulation is repeated with three different instrument designs of various distal length (see Table I). The magnetic field controlled by the user at the center of the eMNS is depicted by the yellow arrow.

and to perform parameter optimization, which has application in the design process of new m-CRs. Once parameter tuning is automatized, parameter optimization performed in simulation promises to be faster and less expensive than fabricating and testing real m-CRs.

Moreover, the contact forces between an m-CR and the vessel wall can be extracted from the simulation, which is an indicator for the invasiveness of the chosen m-CR design. This information is challenging to obtain by conventional means and is usually revealed only late in the m-CR development process.

As computer assistance and automation finds its adoption in robotic assisted surgery, our simulator has the potential to accelerate the development and evaluation of m-CR specific control strategies and human-machine interfaces. Further potential lays in operator training. New adopters can become accustomed to RMN systems more easily by practicing on the simulator. For experienced users, the simulator can be used to practice on particularly challenging anatomies. This can even be patient specific; neuroradiologists can prepare for an intervention by practicing on a patient model based on segmented vessels from preoperative images.

VI. Conclusion

In this work, we presented a simulation platform for m-CRs by coupling the SOFA framework with an eMNS field model, and we validated it experimentally. We demonstrated that the simulation can be used to design and analyze m-CRs and has the potential to be used as a training simulator for physicians.

Acknowledgment

The authors would like to thank Christian Duriez from the DEFROST team and Hugo Talbot from the SOFA Consortium for providing support with the SOFA framework.

References

[1] J. J. Abbott, E. Diller, and A. J. Petruska, "Magnetic Methods in Robotics," *Annual Review of Control, Robotics, and Autonomous Systems*, vol. 3, no. 1, 2020.

[2] J. Bradfield, R. Tung, R. Mandapati, N. G. Boyle, and K. Shivkumar, "Catheter ablation utilizing remote magnetic navigation: a review of applications and outcomes," *Pacing and Clinical Electrophysiology*, vol. 35, no. 8, pp. 1021–1034, 2012.

[3] G. Dabus, R. J. Gerstle, D. T. Cross, C. P. Derdeyn, and C. J. Moran, "Neuroendovascular magnetic navigation: clinical experience in ten patients," *Neuroradiology*, vol. 49, no. 4, pp. 351–355, 2007.

[4] J. Edelmann, A. J. Petruska, and B. J. Nelson, "Magnetic control of continuum devices," *The International Journal of Robotics Research*, vol. 36, no. 1, p. 68–85, jan 2017.

[5] Y. Kim, E. Genevriere, P. Harker, J. Choe, M. Balicki, R. Regenhardt, J. Vranic, A. Dmytriw, A. Patel, and X. Zhao, "Telerobotic neurovascular interventions with magnetic manipulation," *Science Robotics*, vol. 7, p. eabg9907, 04 2022.

[6] S. Zhang, M. Yin, Z. Lai, C. Huang, C. Wang, W. Shang, X. Wu, Y. Zhang, and T. Xu, "Design and characteristics of 3d magnetically steerable guidewire system for minimally invasive surgery," *IEEE Robotics and Automation Letters*, vol. 7, no. 2, pp. 4040–4046, 2022.

[7] S. L. Charreyron, Q. Boehler, B. Kim, C. Weibel, C. Chautems, and B. J. Nelson, "Modeling electromagnetic navigation systems," *IEEE Transactions on Robotics*, vol. 37, no. 4, pp. 1009–1021, 2021.

[8] S. Hoda, A. Tanja, v. d. D. John J., and D. Jenny, "Navigation of guidewires and catheters in the body during intervention procedures: a review of computer-based models," *Journal of Medical Imaging*, vol. 5, no. 1, pp. 1 – 8, 2018.

[9] S. Rahman, C. Thoene, S. Wesarg, and W. Voelker, "Simulation based patient-specific optimal catheter selection for right coronary angiography," in *Medical Imaging 2012: Image-Guided Procedures, Robotic Interventions, and Modeling*, D. R. H. III and K. H. Wong, Eds., vol. 8316, International Society for Optics and Photonics. SPIE, 2012, pp. 838 – 845.

[10] Z. Zhang, J. Dequidt, J. Back, H. Liu, and C. Duriez, "Motion control of cable-driven continuum catheter robot through contacts," *IEEE Robotics and Automation Letters*, vol. 4, no. 2, pp. 1852–1859, 2019.

[11] A. Hong, Q. Boehler, R. Moser, A. Zemmar, L. Stieglitz, and B. J. Nelson, "3d path planning for flexible needle steering in neurosurgery," *The International Journal of Medical Robotics and Computer Assisted Surgery*, vol. 15, no. 4, p. e1998, 2019.

[12] K. See, K. Chui, W. Chan, K. Wong, and Y. Chan, "Evidence for endovascular simulation training: A systematic review," *European Journal of Vascular and Endovascular Surgery*, vol. 51, no. 3, pp. 441–451, 2016.

[13] I. Tunay, "Modeling magnetic catheters in external fields," in *The 26th Annual International Conference of the IEEE Engineering in Medicine and Biology Society*, vol. 1. IEEE, 2004, pp. 2006–2009.

[14] V. K. Venkiteswaran, J. J. Palao, and S. Misra, "A magnetically-steerable stenting catheter for minimally invasive cardiovascular interventions," in *2021 IEEE/ASME International Conference on Advanced Intelligent Mechatronics (AIM)*, 2021, pp. 848–854.

[15] V. N. T. Le, N. H. Nguyen, K. Alameh, R. Weerasooriya, and P. Pratten, "Accurate modeling and positioning of a magnetically controlled catheter tip," *Medical Physics*, vol. 43, no. 2, pp. 650–663, 2016.

[16] Q. Peyron, Q. Boehler, K. Rabenorosoa, B. J. Nelson, P. Renaud, and N. Andreff, "Kinematic analysis of magnetic continuum robots using continuation method and bifurcation analysis," *IEEE Robotics and Automation Letters*, vol. 3, no. 4, pp. 3646–3653, 2018.

[17] R. Zhao, Y. Kim, S. Chester, P. Sharma, and X. Zhao, "Mechanics of hard-magnetic soft materials," *Journal of the Mechanics and Physics of Solids*, vol. 124, pp. 244–263, 2019.

[18] Y. Kim, G. Parada, S. Liu, and X. Zhao, "Ferromagnetic soft continuum robots," *Science Robotics*, vol. 4, no. 33, p. eaax7329, 2019.

[19] C. Zhou, Y. Yang, J. Wang, Q. Wu, Z. Gu, Y. Zhou, X. Liu, Y. Yang, H. Tang, Q. Ling, *et al.*, "Ferromagnetic soft catheter robots for minimally invasive bioprinting," *Nature communications*, vol. 12, no. 1, pp. 1–12, 2021.

[20] L. Wang, C. Guo, and X. Zhao, "Magnetic soft continuum robots with contact forces," *Extreme Mechanics Letters*, p. 101604, 2022.

[21] F. Faure, C. Duriez, H. Delingette, J. Allard, B. Gilles, S. Marchesseau, H. Talbot, H. Courtecuisse, G. Bousquet, I. Peterlik, and S. Cotin, "SOFA: A Multi-Model Framework for Interactive Physical Simulation," in *Soft Tissue Biomechanical Modeling for Computer Assisted Surgery*, ser. Studies in Mechanobiology, Tissue Engineering and Biomaterials, Y. Payan, Ed. Springer, June 2012, vol. 11, pp. 283–321.

[22] C. Duriez, S. Cotin, J. Lenoir, and P. Neumann, "New approaches to catheter navigation for interventional radiology simulation," *Computer aided surgery*, vol. 11, no. 6, pp. 300–308, 2006.

[23] L. Karstensen, T. Behr, T. Pusch, F. Mathis-Ullrich, and J. Stallkamp, "Autonomous guidewire navigation in a two dimensional vascular phantom," *Current Directions in Biomedical Engineering*, vol. 6, no. 1, p. 20200007, 2020.

[24] T. Behr, T. Pusch, M. Siegfarth, D. Hüsener, T. Mörschel, and L. Karstensen, "Deep reinforcement learning for the navigation of neurovascular catheters," *Current Directions in Biomedical Engineering*, vol. 5, no. 1, pp. 5–8, 2019.

[25] S. Guo, X. Cai, Y. Zhao, and B. Gao, "A novel VR-based simulator for the interventional surgical catheter and guidewire cooperation," in *2018 13th World Congress on Intelligent Control and Automation (WCICA)*, 2018, pp. 21–25.

[26] P. Wei, Z. Feng, X. Xie, G. Bian, and Z. Hou, "FEM-based guide wire simulation and interaction for a minimally invasive vascular surgery training system," in *Proceeding of the 11th World Congress on Intelligent Control and Automation*, 2014, pp. 964–969.

[27] M. Quigley, K. Conley, B. P. Gerkey, J. Faust, T. Foote, J. Leibs, R. Wheeler, and A. Y. Ng, *ROS: an open-source Robot Operating System*. ICRA, 2009.

[28] A. J. Petruska, J. Edelmann, and B. J. Nelson, "Model-Based Calibration for Magnetic Manipulation," *IEEE Transactions on Magnetics*, vol. 53, no. 7, 2017.

[29] G. Bradski, "The opencv library." *Dr. Dobb's Journal: Software Tools for the Professional Programmer*, vol. 25, no. 11, pp. 120–123, 2000.

[30] G. Zada, J. Breault, C. Liu, A. Khalessi, D. Larsen, G. Teitelbaum, and G. S.L., "Internal carotid artery aneurysms occurring at the origin of fetal variant posterior cerebral arteries: surgical and endovascular experience," *Neurosurgery*, vol. 63, 2008.

[31] M. Beppu, Y. Kuramoto, S. Abe, S. Namitome, and S. Yoshimura, "Localized kinking during deployment of a flow redirection lumen device (fred) could be due to excessive pushing," *Surgical Neurology International*, vol. 13, p. 22, 01 2022.

[32] M. P. Kummer, J. J. Abbott, B. E. Kratochvil, R. Borer, A. Sengul, and B. J. Nelson, "Octomag: An electromagnetic system for 5-dof wireless micromanipulation," *IEEE Transactions on Robotics*, vol. 26, no. 6, pp. 1006–1017, 2010.